IJHSR
ijhighschoolresearch.org
RESEARCH ARTICLE

Magneto-Optical Kerr Effect Measurements of In-Plane Anisotropies in Ni/Au and Ni/Al_2O_3 Thin Films

Jeet Bhatnagar, Ethan Liu, Will Davitt, James Liu, Katie Driscoll

Hopkins School, 986 Forest Rd, New Haven, CT, 06515, USA; jeetbhatnagar3@gmail.com
Mentor: Priscilla Encarnacao, Benjamin Taylor

ABSTRACT: The study used the magneto-optical Kerr effect (MOKE) in longitudinal and polar configuration to measure hysteresis loops of thin Au and Al_2O_3-capped Ni films to compare the axial preference of anisotropies in the magnetization of these films. To assess these features, samples were rotated azimuthally, measuring the Kerr angle as a function of the applied field for each recorded azimuthal angle. The remanence and coercivity depicted in the Al_2O_3-capped and the Au-capped samples' hysteresis loops decreased monotonically as a function of the azimuthal angle over the instrumental range in a cycloid-like shape. Both samples' easy axes contained a similar shape and coercivities (Au-capped H_c: 11.76 ± 1 Oe, Al_2O_3-capped H_c: 10.78 ± 1Oe). In contrast, the hard axes of both samples presented different shapes, with the Al_2O_3-capped sample's hysteresis loop portraying two distinct spikes. These spikes represent return transitions—abrupt changes in magnetization during reversal—potentially resulting from DMI, shape anisotropies, oxidation, training effects during Ni film deposition, or other coupling effects with the Al_2O_3 cap layer.

KEYWORDS: Physics and Astronomy; Atomic, Molecular, and Optical Physics; Anisotropy, MOKE; DMI.

Introduction

Anisotropies in magnetic thin films are of significant interest to solid-state physics and engineering communities due to their applications in information storage devices.[1] Controlling magnetic moments along specific axes helps regulate magnetization behavior. Magnetic anisotropies can be induced through various mechanisms, including shape-influenced finite-size effects, substrate lattice strain, and spin-orbit coupling interactions in multilayer heterostructures.[2] The specific structure and composition of the film determines in-plane preferences.[3]

It is well-established that thin nickel (Ni) films typically exhibit in-plane anisotropies.[4-6] This is often due to training during film deposition, which naturally aligns the magnetic easy and hard axes. Any piece of Ni, regardless of size, will exhibit a hard and easy axis somewhere due to these effects. However, shape anisotropies, exposure to oxidation, and other factors can also influence anisotropy. Additionally, some studies have demonstrated that an Au overlayer can induce an out-of-plane anisotropy in a thin Ni film through spin-orbit coupling driven by Dzyaloshinskii-Moriya interactions (DMI).[7] DMI arises due to the lack of inversion symmetry at the crystal lattice or material interface,[8] as seen in Ni/Au bilayer films. These interactions can lead to strong spin-orbit coupling, forming low-dimensional structures with in-plane orientations.[9]

The crystallinity of the Ni films in this study is likely polycrystalline with small grain sizes, which contributes to the observed magnetic anisotropy within the film. Despite the film being crystalline-isotropic at the macro scale, the small grains introduce a preferred in-plane anisotropy, leading to directional dependence in magnetization. This effect between film structure and anisotropy is further complicated by the spin-orbit interactions, which affect the magnetization response, especially in the presence of interfacial layers like Au or Al_2O_3.

This study builds on these foundational concepts by focusing specifically on how anisotropy in thin magnetic films is influenced by this interplay between spin-orbit coupling and film structure. While earlier studies have observed anisotropies in Ni films with various capping materials, the effects of DMI on the precise nature of in-plane and out-of-plane components have not been rigorously characterized. By carefully investigating hysteresis loops under azimuthal rotation, this work aims to clarify the contribution of DMI to magnetic anisotropy in Ni/Au and Ni/Al_2O_3 bilayers. Understanding how these interactions manifest in the measured magnetic response will provide deeper insight into the mechanisms driving anisotropic behaviors in magnetic thin films, which are critical for designing materials in applications like data storage.

In previous studies, as discussed by Dr. Moodera,[7] while testing the longitudinal hysteresis in the associated samples, some anisotropy in the in-plane response was detected but not rigorously characterized. In this present study, the samples under azimuthal rotation were further investigated to check for in-plane anisotropies carefully using the Magneto-Optic Kerr Effect (MOKE), acquiring hysteresis loops for a 20 nm Ni film grown on glass and capped with either 4 nm of Au or Al_2O_3 respectively. Longitudinal experimental geometry was employed to determine the axial preference in the magnetization of our thin films. The Al_2O_3-capped control should exhibit an in-plane preference, consistent with prior research done by Kang *et al.*[4]

MOKE is characterized by a rotation in the linear polarization of light upon reflection from a magnetic material.[10] Linearly polarized light combines left- and right-hand circu-

  DOI: 10.36838/v7i4.92

larly polarized beams. The magnetization (**M**) of the material asymmetrically affects the off-diagonal elements of the dielectric tensor, creating different indices of refraction for each circular polarization.[11] Upon reflection from a magnetized surface, the light undergoes a complex rotation of polarization, known as the Kerr angle, proportional to **M**.[11] The magnitude of this rotation is also proportional to the dot product of the Poynting vector and the magnetization direction, that can be exploited in various experimental geometries.[11]

Figure 1 shows how an external magnetic field is used to drive moments in the sample while recording intensity variation of the beam after passing through an analyzing polarizer, resulting in hysteresis loops.

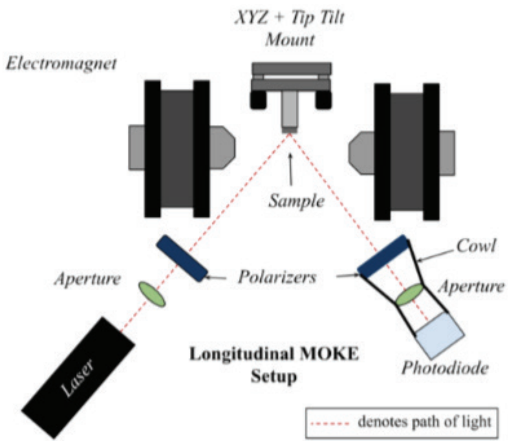

Figure 1: Image of longitudinal MOKE sample setup, showing labeled individual parts of the apparatus.

The orientation of the optical plane and applied magnetic field allows for several experimental geometries, including longitudinal (where the applied field lies in the film plane), as shown below in Figure 2a and polar (where the field is instead applied perpendicular to the film surface), as shown below in Figure 2b. Each yields a hysteresis curve corresponding to the magnetic moment in the direction of the applied field, thus demonstrating whether hysteresis exists in-plane and out-of-plane. This study used the longitudinal orientation to make initial observations about the specific longitudinal hysteresis, and then polar to further verify and interpret those results.

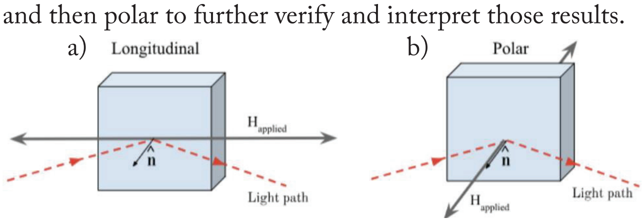

Figure 2: Image of longitudinal (Figure A) and polar (Figure B) MOKE sample orientations, showing the orientations of the sample in relation to the light path.

To analyze the anisotropy characteristics of our samples, the coercivities, recorded as a function of field orientation – referred to as the azimuthal angle – of both samples could be used to determine differences in the impact of DMI, shape anisotropies, and exposure to oxidation throughout both samples, which can then be verified by observing the anisotropy fields of the respective samples. To find this anisotropy field, the Stoner-Wolfarth model was used. The Stoner-Wohlfarth model, depicted below in Equation 1, represents the theoretical field required to reverse magnetization through coherent rotation under an external field, predicting the switching field H_s as a function of the applied field angle, where H_a correlates to the anisotropy field.

$$\text{Equation 1: } H_s = H_a\left(\cos^{\frac{2}{3}}\theta + \sin^{\frac{2}{3}}\theta\right)^{-\frac{3}{2}}$$

However, in experimental hysteresis measurements, the coercive field H_c is defined as the field at which the magnetization crosses zero, which can deviate from H_s due to defects within the metal. For the purpose of experimentally determining the anisotropy field, the angular dependence of $H_c(\theta)$ can be approximated using a quadratic sine dependence, yielding the modified expression depicted below in Equation 2.

$$\text{Equation 2: } H_c(\theta) = H_{c0} + H_a \sin^2(\theta - \theta_0)$$

Within Equation 2, H_{c0} represents the baseline coercivity, H_a represents the anisotropy field, and $(\theta-\theta_0)$ accounts for the offset from the baseline coercivity position. By fitting experimental coercivity measurements to this equation, the anisotropy field can be extracted, providing insight into the material's magnetic anisotropy and its angular dependence.

During this experiment, variations in remnant magnetization and coercive field as a function of azimuthal angle ($\theta_{azimuth}$) up to 90 degrees are expected, revealing characteristics of the in-plane magnetic anisotropy for both samples. However, the effects of DMI are expected to appear in the measured magnetic hysteresis, influencing the anisotropy and potentially indicating deviations from purely in-plane magnetization behavior.

Additionally, magnetization reversal in the Al_2O_3-capped sample may exhibit return transitions—sudden changes in magnetization during hysteresis, potentially arising from domain wall pinning or interfacial coupling.

Materials and Methods

Because MOKE measures optical intensity variation due to small polarization shifts, the light source, sample mounts, and polarizers are critical elements for controlling and optimizing the signal-to-noise ratio. To that end, a 635nm, 5mW Power Technologies (model PPM (635-5)G38) intensity stabilized laser and Glan-Thompson polarizers (extinction ratio of ~10^{-5}) in micrometer-driven rotation mounts (0.1° resolution) were used. The optical intensity was measured via a Thorlabs SMO5PD2A silicon photodiode (used with a 0.3nA dark current), Thorlabs PDA200C preamp, and a National Instruments USB-6341 I/O board read by a custom LabView interface. The magnetic field was generated using two magnets: 1. For large fields greater than 100 Oe, a GMW-3470 electromagnet, and 2. For the larger angle of incidence and improved signal-to-noise ratio, a hand-wound electromagnet uses fields up to 100 Oe. Each was powered by a KepCo BOP 50-8m bipolar power supply controlled by the aforementioned I/O board and software. A PASCO PS2162 2-axis field probe and a PASCO 850 instrument interface to monitor the magnetic field created by the electromagnets.[6]

The azimuthal angle ($\theta_{azimuth}$) is defined such that $\theta_{azimuth} = 0°$ corresponds to the in-plane field aligned parallel to the sample's reference edge, with positive $\theta_{azimuth}$ increasing counterclockwise when viewed from above. The Kerr Angle at each scan point is determined by measuring the intensity variation through a fixed analyzer position, calibrated beforehand to optimize sensitivity to magnetization changes.

The Ni/Au film sample was grown for study by the Moodera research group at MIT. The samples shown in Figure 3 were made in an Ultra-High Vacuum thin film deposition system in which Ni was evaporated using an electron gun source while the Au was grown via a tungsten boat source. The film growth rate was measured using a quartz crystal monitor.[7]

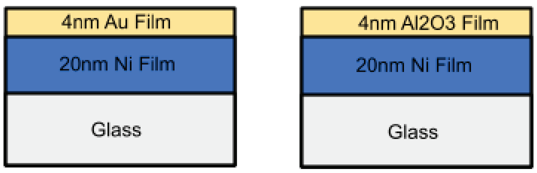

Figure 3: Sample cross sections of Au and Al_2O_3-capped Ni. Both comprise a 20nm Ni film layer on a glass substrate, capped with a 4nm layer of Au and Al_2O_3, respectively.

Result and Discussion

Longitudinal MOKE scans were performed on the aforementioned samples at room temperature in air, yielding the hysteresis loops shown below, in Figures 3a and 3b, by the rotations in their respective Kerr angles.

a) b)

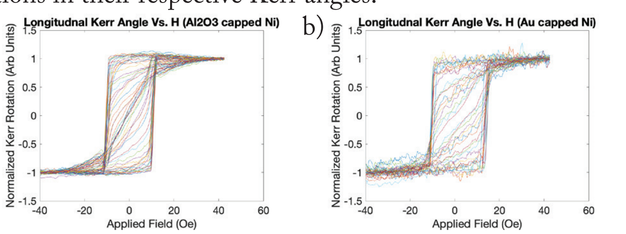

Figure 4: Longitudinal hysteresis loops of Al_2O_3 (Figure A) and Au-capped Ni (Figure B) with varying $\theta_{azimuth}$. Both samples showed a gradual shift from ferromagnetic to paramagnetic behavior as the sample was rotated. Figure A contains 19 traces, 5 degrees apart, representing the transition from $\theta_{azimuth}$ from 0 to 90 degrees. Figure B contains 18 traces, 5 degrees apart (with the last trace 3 degrees apart), representing the transition from $\theta_{azimuth}$ from 0 to 83 degrees. Figure B was not carried out to 90 degrees due to data limitations but the trend was still observable.

First, the change in the hysteresis of both Al_2O_3 and Au-capped Ni samples over the change in their Kerr angles was examined; both figures show how the hysteresis loops converged to a near-zero remanence percentage as the sample was rotated up to about 90°.

a) b)

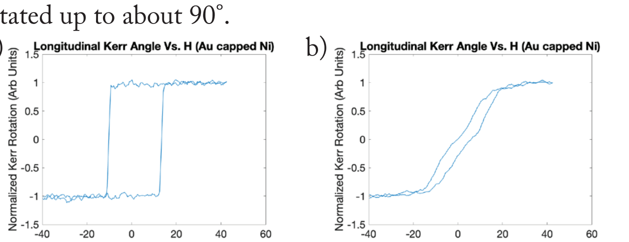

Figure 5: Comparing the longitudinal hysteresis easy (Figure A) and hard axes (Figure B) for Au-capped Ni. The easy axis displays square ferromagnetic hysteresis, while the hard axis displays gradual anisotropic change and paramagnetic behavior.

Longitudinal MOKE scans of the easy and hard axis of the Au-capped sample were then performed at room temperature in air, yielding the two hysteresis loops shown in Figures 5a and 5b above. The easy axis graph depicts a sharp hysteresis loop with near 100% remanence and coercivity (H_c) of 11.76±1 Oe. Meanwhile, the hysteresis loop of the hard axis shows a much more gradual change of the in-plane anisotropies within the sample as a function of the applied field, with a remanence of around 16.04% and a coercivity (H_c) of 3.04 ± 1 Oe. This data, as well as in Figure 4, shows how the coercivity of the in-plane anisotropy of the Au-capped sample seemed to change uniformly as a function of the azimuthal angle.

Additionally, with Figure 5b, a double step hysteresis loop can be observed, suggesting that magnetization does not reverse smoothly but instead occurs in two distinct stages. This could be due to variations in local strain or defects within the Ni film, causing different regions to switch at slightly different applied fields. Furthermore, the Au capping layer may influence the magnetic properties by modifying the energy landscape at the interface, affecting how the material responds to the applied field. These results highlight the effect of Au capping on magnetization reversal and coercivity. To further explore the role of capping layers, similar longitudinal MOKE scans were performed on an Al_2O_3-capped Ni sample at room temperature in air, as shown in Figures 6a and 6b below.

a) b)

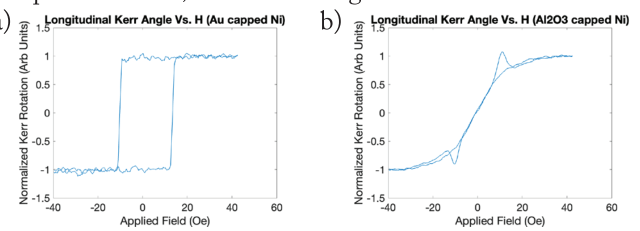

Figure 6: Comparing the longitudinal hysteresis easy (Figure A) and hard (Figure B) axes for Al_2O_3-capped Ni. The easy axis displays square hysteresis, which is similar to Au-capped samples. The hard axis resembles Au-capped except for two return transitions.

Figure 6 compares the longitudinal hysteresis loops of the easy (Figure 6a) and hard (Figure 6b) axes for the Al_2O_3-capped Ni sample. The easy axis shows a sharp hysteresis loop with near 100% remanence, similar to the Au-capped samples, and coercivity of 10.78 ± 1 Oe. The hard axis loop is similar to the Au-capped sample, but with two distinct return transitions, clearly visible in Figure 6b. These transitions occur on the return path of the hysteresis loop as the applied field is swept back, and they may be influenced by effects such as DMI, shape anisotropies, or differential oxidation exposure during the deposition process, particularly when compared to the Au-capped sample.

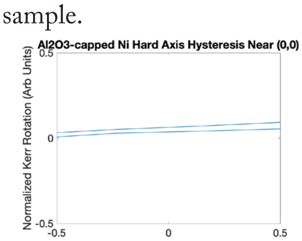

Figure 7: Zoomed-in view of the hard-axis hysteresis loop for the Al_2O_3-capped Ni sample, highlighting the region around (0,0) to better illustrate the lack of coercivity and remanence.

DOI: 10.36838/v7i4.92

Figure 7 presents a zoomed-in view of the hard-axis hysteresis loop from Figure 6b, focusing on the region around (0,0) to clarify the coercivity and remanence. Much like the Au-capped sample, the remanence and coercivity of the Al_2O_3-capped sample decreased drastically due to the change in the azimuthal angle, with a remanence of 4.86% and coercivity (H_c) of 0.68 ± 1 Oe at a 90-degree rotation.

Figure 7 further shows how the return path of the hysteresis loop closely follows the forward path, suggesting close to zero coercivity, with the measured value being 0.68 Oe. Additionally, the hysteresis loop's near passage through the point (0,0) is indicative of a possible zero remanent field, with a value close to the measured 4.68%.

Additional simulations were performed outside this experiment using mumax3 with the same Al_2O_3-capped Ni sample yielding similar hysteresis for the hard axis, as shown in Figure 8 below.[12] The simulations were performed with a Dell computer with an Intel core i7-10700 2.9ghz CPU and an Nvidia GeForce GTX 1660 SUPER GPU with 16 GB RAM. The grid dimensions were 192 nm by 192 nm by 15 znm with 5 layers of Ni simulated. The applied field was simulated from 800 to -800 and back to 800 mT in increments of 1 mT. The saturation magnetization of the Ni was given to be 485 kA/m. Simulation conditions also included an exchange stiffness of 10 pJ/m between the Ni layers and a constant DMI strength of 1 mJ/m^2, used to represent the interaction between the Ni and Al_2O_3 layers.

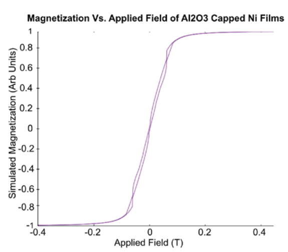

Figure 8: Simulation of longitudinal hysteresis hard axis (Al_2O_3-capped Ni). Resembles hard axis of Al_2O_3-capped Ni, displaying distinct return transitions.

This graph, with similar return transitions to Figure 6b, suggests that a probable cause of the return transitions in the Al_2O_3-capped Ni sample was the DMI between the bilayers of this heterostructure, forcing out-of-plane anisotropy of magnetic moments in the sample.

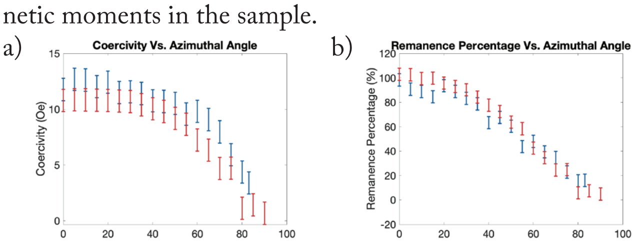

Figure 9: Dependence of coercivity (Figure A) and remanence percentage (Figure B) on an azimuthal angle (blue represents Au-capped while red represents Al_2O_3-capped). Both coercivity and remanence decrease with downward concavity as a function of azimuthal angle. While the Al_2O_3-capped sample was rotated to 90 degrees, the Au-capped sample was only rotated to 83 degrees due to data limitations – which was still deemed sufficient to observe the trend.

Using the data collected from the longitudinal MOKE scans above, the coercivity and remanence percentages of each sample's hysteresis were graphed as a function of their azimuthal angle, depicted in Figures 9a and 9b above. In both graphs, a general trend of the coercivity and remanence percentage decreasing as the sample was rotated to an azimuthal angle of 90 degrees is present, with the coercivity and remanence percentages of both seeming to decrease in the shape of a cycloid. This is persistent with the initial hypothesis of coercivity and remanence percentages of both samples clearly decreasing with downward concavity as a function of their respective azimuthal rotations.

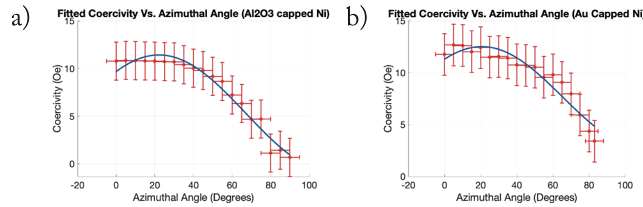

Figure 10: Fitting the data of the coercivity as a function of the azimuthal angle for the Al_2O_3 –capped (Figure A) and NiAu-capped (Figure B) films respectively, to Equation 2. The error bars depicted above on each data point represent ±5° on the x-axis, and ±2 Oe on the y-axis. The correlation between the best fit line and the data for Figure 10a was determined to have R^2 = .97, and for Figure 10b, a value R^2 = .92.

The data for the coercive field as a function of the azimuthal angle found in Figures 9a and 9b was further used to determine the anisotropy field surrounding the capped samples to make further observations around the magnetization of the films. Figure 10a outputs a value of 12.2 Oe for the anisotropy field, whereas Figure 10b yielded a value of 9.8 Oe.

The difference in anisotropy field values between the two capped samples suggests that the choice of capping material influences the magnetic properties of the underlying films. The higher anisotropy field of 12.2 Oe in Figure 10a indicates stronger resistance to magnetization rotation, which could result from increased strain, interfacial exchange interactions, or enhanced surface anisotropy, consistent with the return transitions observed in Figure 6b. In contrast, and consistent with the absence of return transitions in Figure 5b, the lower anisotropy field of 9.8 Oe in Figure 10b suggests a reduction in these effects, potentially due to differences in interfacial spin-orbit coupling or modifications in magneto crystalline anisotropy.

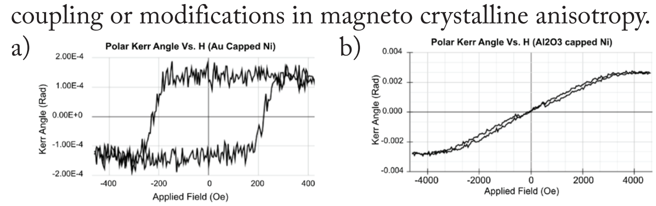

Figure 11: Polar scans of the performed MOKE on Au-Capped (Figure A) and Al_2O_3-capped (Figure B) samples.

To further explore the magnetic preferences of the samples, we then examined the polar scan of the Au-capped sample shown above in Figure 11a; the MOKE signal in polar configuration depicts a clear, wide hysteresis loop with near 100% remanence, and a coercivity (H_c) of ~230 ± 10 Oe - there was a slight slope to the loop, possibly due to some complex domain structures, that was removed to isolate the ferromagnetic com-

DOI: 10.36838/v7i4.92

ponent. The presence of strong remnant hysteresis (though vastly different H_c to longitudinal measurements in Figure 5a found to be 11.76 ± 1 Oe) in both polar and longitudinal orientations may suggest a hybrid domain structure with, perhaps, out of plane preference near the Au interface, and in-plane preference deeper in the film towards the glass substrate.

Figure 11b then shows the MOKE signal in polar configuration corresponding to the Al_2O_3-capped sample, which depicts a paramagnetic response with near-zero remanence and coercivity. The MOKE signal in longitudinal configuration generated a reasonably square hysteresis loop with near 100% remanence and a coercivity of 10.78 ± 1 Oe, shown in Figure 6a. This difference suggests an in-plane preference with a weak coercivity–this agrees with prior work on Ni thin films and stands in direct contrast with the results from our Au-capped film.

Conclusion

The goal of the study was to compare the hysteresis of Au-capped Ni films with Al_2O_3-capped Ni films to determine the coercivity and remanence percentage of the orientation of the in-plane anisotropy within those films as a function of the angle they were rotated to around the azimuthal axis. Initially, a DMI presence in Au-capped Ni samples was expected to occur, along with a general trend of decreasing coercivity and remanence percentages for both samples as they were rotated azimuthally to the hard axis. Longitudinal scanning found that anisotropies were uniaxially in-plane for both samples, all with orientations producing remanence and non-zero coercive field. In both samples, the coercivity and remanence were found to decrease as a function of the azimuthal angle from 0 to 90 degrees [(Au-capped H_c: 11.76 ± 1 Oe → 3.04 ± 1 Oe, Remanence: 98.35% → 16.04%), (Al_2O_3-capped H_c: 10.78 ± 1 Oe → 0.68 ± 1 Oe, Remanence: 100.00% → 4.86%)]. However, the remanence of the Au-capped sample seemed to contrast in its shape, comparative to the decrease in the remanence of the Al_2O_3 samples, perhaps suggesting different DMI, shape anisotropy, or other coupling effects present in both samples. Additionally, hysteresis loops in a polar configuration were examined to further reveal out-of-plane anisotropy for our Au capped sample (Polar: H_c ~230 Oe), in contrast to the behavior of our Al_2O_3 capped sample which had a near paramagnetic response in the polar direction and a ferromagnetic hysteresis loop in the longitudinal direction with a coercivity of 11.76 ± 1 Oe. The similarity of the in-plane responses from each sample may suggest that the Au-capped film has some depth dependence in its behavior: perhaps deeper layers within the Ni film still behave like those in the Al_2O_3 capped film, while layers close to the Au interface are being pulled out of plane.

Furthermore, the hysteresis of the Al_2O_3-capped sample was different than initially expected due to the presence of return transitions, likely also suggesting the presence of DMI, shape anisotropies, or the effect of oxidation during the Ni film training deposition within the sample. However, the return transition observed in the Al_2O_3-capped sample suggests a possible contribution from DMI, which contrasts with the expectation that the Au cap would be the primary source of such effects. This indicates an additional or alternative mechanism at play, potentially representing a novel finding that warrants further investigation. This suggestion is further supported by the simulation results and differences in the anisotropy fields for the Au- and Al_2O_3-capped samples. These differences point more directly to the presence of DMI, variations in spin-orbit coupling, or, more generally, differences in the metal properties themselves as the cause of the observed return transitions in the Al_2O_3-capped samples. In contrast, the absence of such return transitions in the Au-capped samples suggests that DMI or other effects may not be as pronounced in the Au-capped sample, or that different underlying mechanisms, that would warrant further study, are at play in these materials.

To further explore the differences in the in-plane anisotropies of Au and Al_2O_3-capped Ni samples, another simulation could be run with increased and decreased DMI constants on both samples to try and identify a more precise correlation between DMI's presence within the sample and irregular trends in the hysteresis loops of the sample. More specifically, it would be of interest to identify whether the return transitions observed in Figure 6b always occur within Al_2O_3-capped Ni samples, and to see if they ever occur within MOKE performed on Au-capped samples, through performing MOKE on other Au and Al_2O_3-capped Ni samples. Additionally, to more directly prove the effects of DMI within the experiment, saturation magnetization of the sample can be explored using different techniques like VSM (Vibrating Sample Magnetometer) and SQUID (Superconducting Quantum Interference Device Magnetometer). Furthermore, to improve the data gathered above, the Au-capped Ni scans could be completed out to 90 degrees rather than stopping at 83 degrees, and the electromagnet itself could be made smaller to create better control over the angle of incidence and enhance the overall MOKE signal strength and the signal-to-noise ratio, while also further eliminating noise that impactfully contributes to the results of the study.

Declaration of use of AI in this work

Because this research was performed exclusively by high school-level students at our institution, students used OpenAI's ChatGPT and Google's Gemini to help summarize and simplify reference articles. After using these tools, the authors reviewed and edited the content as needed and took full responsibility for the publication's content. No generative AI tool was used to produce data, plots, or interpret results.

Acknowledgments

We offer many thanks to Professor Jagadeesh Moodera at MIT for supplying samples and inspiration to pursue this study, Professor Boris Sinkovic of UConn for continued help supporting this high school laboratory, and the He and Schiffer Laboratories at Yale University, who supplied advice and help along the way.

DOI: 10.36838/v7i4.92

References

1. Yale University School of Engineering & Applied Science. (n.d.). “Hard Drives Methods And Materials,” Retrieved from https://volga.eng.yale.edu/teaching-resources/hard-drives/methods-and-materials.
2. J. Camarero, J.J. de Miguel, R. Miranda, V. Raposo, A. Hernando. (2001); "Influence of Flm Morphology on Perpendicular Magnetic Anisotropy." Physical Review B, Vol. 64, 125406.
3. Fernando, G. W., In Handbook of Metal Physics, Vol. 4, 89–110 (Elsevier, 2008).
4. S. S. Kang, X. Y. Liu, X. H. Xiang, G. J. Jin, J. H. Du, M. Lu, et al. (1998); "Growth-induced magnetic anisotropy behavior in Ni thin films," J. Magn. Magn. Mater., vol. 187, pp. 154.
5. Rattanasakulthong, W., Sirisangsawang, P., Pinitsoontorn, S. & Sirisathitkul, C (2011); Dependence of hysteresis loops on thickness of thin nickel films prepared by RF sputtering. Adv. Mat. Res 335-336, 1443–1447.
6. V. Aryan, P. Ivanov, B. Kaduboski, N. Kargin, N. Lee, J. Mao, V. Montresoro, F. Polak, I. Slattery, P. Encarnacao, B. Taylor (2023); Magneto Optic Kerr Effect Measurements of In-Plane-Out-of-Plane Anisotropies Induced by Spin-Orbit Coupling Effects in a Ni/Au Thin Film.
7. Moodera, J. (Private Communication, March 2020).
8. Qihan Zhang, Jinghua Liang, Kaiqi Bi, Le Zhao, He Bai, Qirui Cui, Heng-An Zhou, Hao Bai, Hongmei
9. Feng, Wenjie Song, Guozhi Chai, O. Gladii, H. Schultheiss, Tao Zhu, Junwei Zhang, Yong Peng, Hongxin Yang, & Wanjun Jiang (2022); Quantifying the Dzyaloshinskii-Moriya Interaction Induced by the Bulk Magnetic Asymmetry. Physical Review Letters, 128 (16).
10. Robert E. Camley, Karen L. Livesey (2023); Consequences of the Dzyaloshinskii-Moriya interaction. Surface Science Reports, Volume 78, Issue 3.
11. Thorne, K.S., Blandford, R.D. (2017); Modern Classical Physics: Optics, Fluids, Plasmas, Elasticity, Relativity, and Statistical Physics. Princeton, NJ: Princeton University Press (Digital file).
12. Z.Q. Qiu, S.D. Bader (2000); Rev. Sci. Inst. 71, 1243.
13. J. Liu, K. Driscoll, B. Taylor, P. Encarnacao (2024); Simulating Dzyaloshinskii-Moriya Interactions in Ni/Au and Ni/Al_2O_3 Thin Films with Mumax3.

Authors

Jeet Bhatnagar, Ethan Liu, James Liu, Will Davitt, and Katie Driscoll are high school seniors at Hopkins School in New Haven, CT. They are passionate about applied physics, particularly magnetic anisotropy, which they explored through a school research program. Their interests in physics and engineering deepened through independent research projects and internships in professional laboratory settings during their high school careers.